



Title	Optical properties of chalcogen-loaded zeolite (ZSM-5)
Author(s)	Saitoh, Akira; Tanaka, Keiji
Citation	Solid State Communications, 149(19-20), 750-753 https://doi.org/10.1016/j.ssc.2009.03.007
Issue Date	2009-05
Doc URL	http://hdl.handle.net/2115/38591
Type	article (author version)
File Information	149-19-20_p750-753.pdf



[Instructions for use](#)

Optical properties of chalcogen-loaded zeolite (ZSM-5)

Akira Saitoh, Keiji Tanaka

Department of Applied Physics, Graduate School of Engineering, Hokkaido University, Sapporo, 060-8628, Japan

Corresponding author: Keiji Tanaka. Address: Department of Applied Physics, Graduate School of Engineering, Hokkaido University, Sapporo, 060-8628, Japan. Tel: +81-11706-6630; fax: +81-11-706-6859.

E-mail address: keiji@eng.hokudai.ac.jp

Abstract

Sulfur, selenium, and tellurium were loaded into sub-mm size ZSM-5 single crystals and the optical properties have been comparatively studied. S and Te show similar features, while Se is unique. S and Te have optical absorption edges at wavelengths of ~ 400 nm with transmission dips at ~ 450 nm, while Se has the edge at ~ 550 nm. The three materials provide photoluminescence at visible wavelengths, with intensities of S and Te being stronger than that of Se by two orders. These optical properties imply that S and Te in the zeolite form small atomic units such as S_3 and Te_2 , while Se condenses into single-chain structures.

Keywords: A. Chalcogen, A. Zeolite, C. Single chain, D. Photoluminescence

(for A. Types of Materials; B. Preparation and Processing; C. Structure and characterization; D. Phenomena and properties; E. Experimental methods)

1. Introduction

Studies on nano-structured materials attract growing interest [1]. Here, the zeolite, a porous crystal with typical compositions of Al-Si-O having varied (more than 100 kinds [2]) structures, has been demonstrated to work as a good matrix for producing well-defined nano-structures [3]. And, a lot of researches have been reported for a variety of combinations of a zeolite and a guest element, which may be organic [3-5], inorganic [6], or metallic [3]. Among those, pioneering work by Bogomorov et al. has demonstrated that a chalcogen behaves as an interesting guest [7-9], partly because the chalcogen forms molecules with ring and chain structures, which may not produce many dangling bonds when nano-structured. Substantial successive studies have been published [10-19].

However, most of previous studies on chalcogen-loaded zeolites are limited in three respects. First, as summarized in Fig. 1, the pore size of employed zeolites has been 0.3-1.2 nm in free diameter, which may be substantially greater than typical sizes of chalcogen atoms and molecules [11, 19]. (The free diameter is calculated from a framework diameter, a pore distance between atom cores, and an ionic diameter, ~ 0.27

nm, of oxygen [2].) Second, Al/Si ratios in the zeolites have been 0.2-1 (Fig. 1), being more-or-less polar, which is likely to exert substantial ionic effects to covalent chalcogen molecules [11, 17, 18], as theoretically predicted [20]. Third, many of previous studies, with a few exceptions [14-16, 19], have employed powder-like zeolites with typical sizes of $\sim 1\ \mu\text{m}$ [7, 9, 10, 12, 13]. Accordingly, chalcogens deposited onto the surface of zeolites may modify or govern measured properties. In addition, the powder-like zeolite can afford to investigate only ensemble-averaged properties, making difficult to know single-crystalline properties. Powder-like materials also produce substantial light scattering, which is likely to mask optical absorption spectra.

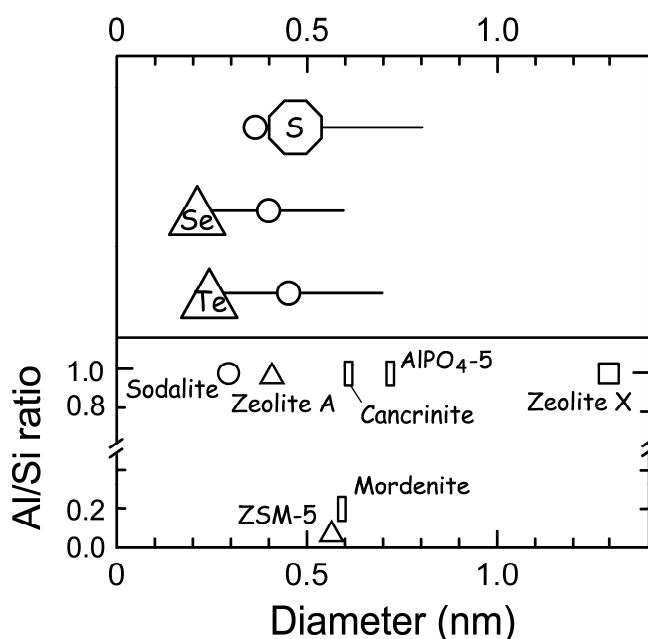


Fig. 1. A list of zeolite of interest and chalcogen. In the lower part, the zeolite is specified by the Al/Si ratio (or Al/P for $\text{AlPO}_4\text{-5}$) and the free pore diameter with symbols representing conformation dimensions of pore structures; a spherical cavity by a circle, one-dimensional channels by rectangles, a two- by a square, and the three- by triangles. In the upper part, van-der-Waals diameters of chalcogen atoms (circles) and sizes of related molecules are depicted. For S, a framework diameter of S_8 ring molecule is plotted with an attached bar extending to an approximate size taking a van-der-Waals atomic diameter into account. For Se and Te, framework cross-sectional diameters of the three-fold helices in trigonal crystals are plotted with the bars to the van-der-Waals diameters.

Accordingly, for examining reliable properties of nano-structured chalcogens, we should select a zeolite, at least, on three conditions. First, the pore size should preferably be comparable to the size of incorporated atomic clusters. Second, the external shape should be regular and single-crystalline with sub-mm sizes. Smaller and irregular zeolites produce surface effects and light scattering. In contrast, if the size is too large, chalcogen incorporation into the sample may be limited only near the surfaces. Third, the zeolite should be non-polar for suppressing ionic effects.

We here try to impregnate chalcogens (S, Se, Te) into ZSM-5, a kind of MFI zeolites [24-26]. ZSM-5 contains two kinds of channels (see, Fig. 3); the one being nearly straight along the crystalline b axis and the other being roughly zig-zag in the a - c plane, the both having nearly the same framework and free diameters of ~ 0.83 nm and ~ 0.56 nm. The zeolite can be prepared in sub-mm sizes [26], which is appropriate to optical studies. And, as is known, the typical composition is $\text{Si}_{94}\text{Al}_{12}\text{O}_{192}$, being fairly non-polar. We try to incorporate S, Se, and Te into ZSM-5 crystals, and the chalcogen-loaded samples, which will be abbreviated as z-S(Se, Te), are comparatively investigated.

2. Experimental

Chalcogen-loaded samples were prepared as follows: Single-crystalline ZSM-5 with a typical dimension of $\sim 40 \times 40 \times 200 \mu\text{m}^3$ was prepared by Kiyozumi, the procedure being similar to that in Ref.[26]. The ZSM-5 crystal contained organic templates, which were desorbed by a heat treatment at 500°C for 3 h in vacuum just before chalcogen loading. The desorption was confirmed through disappearance of infrared absorption peaks at 1450 and 3000 cm^{-1} , as shown in Fig. 2. Then, piles of ZSM-5 (~ 5 mg) and chalcogen chunks with 6N-purity were vacuum-sealed in a double-arms quartz ampoule, which was heated so that the chalcogen was impregnated from vapor phases into the zeolite. The temperatures and durations, which were selected after several trials for producing dense-colored samples as possible, were 180°C and ~ 10 h for S, 300°C and ~ 3 h for Se, 550°C and ~ 2 h for Te ($T_m = 113^\circ\text{C}$ for S, 217°C for Se, 450°C for Te), where the host zeolites being kept at $\sim 150^\circ\text{C}$. As reported previously [26], in these thermal treatments, slow ($< 30^\circ\text{C/h}$) heating and cooling were needed for suppressing formation of cracks, which made the zeolite smoggy.

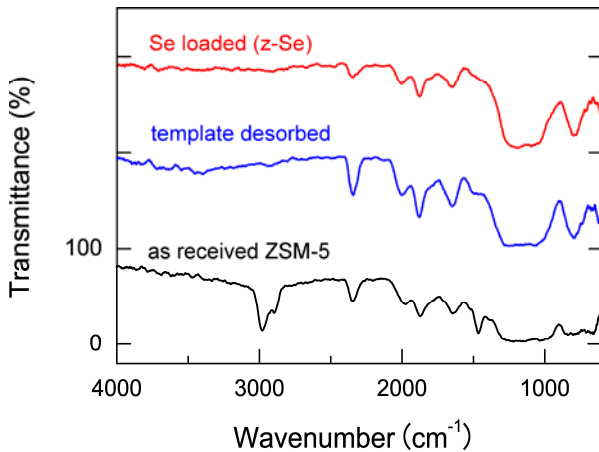


Fig. 2. Infrared spectra of as-received and template-desorbed ZSM-5 and z-Se.

Optical transmission spectra for single samples were obtained using a double-beam spectrometer (JASCO, V-570S). A sample was put on to an aperture with a diameter of $25 \mu\text{m}$, and probe light was transmitted along the a -axis with a length of $\sim 40 \mu\text{m}$. Photoluminescence (PL) was monitored under a reflection arrangement using Ar^+ (488 and 515 nm) and He-Ne (633 nm) lasers, which provided excitation

light with an intensity of $\sim 50 \mu\text{W}$ per spot with a diameter of $\sim 1 \mu\text{m}$, and a detection system consisting of a triple spectrometer (Jobin Yvon, T64000) and a cooled charge-coupled device. Spectral response of the detection system was calibrated using a black-body radiation. In all the present optical measurements, polarization was un-analyzed.

In addition to these measurements, Raman-scattering spectroscopy and x-ray diffraction of chalcogen-loaded samples were examined, while meaningful and comparative results could not be obtained, despite repeated trials. In brief, in z-S and z-Te, Raman scattering spectra were masked by intense PL signals (Fig. 5). On the other hand, X-ray diffraction patterns of z-S showed only peaks arising from ZSM-5. X-ray diffraction for z-Te detected, in addition to some zeolite peaks, at least six peaks, which could be assigned to crystalline Te and TeO_2 . For z-Se, the details will be reported elsewhere.

3. Results

Figure 3 gives a schematic view of ZSM-5, containing magnified channels, and photographs of ZSM-5, z-S, z-Se, and z-Te. We see in the photographs that a transparent ZSM-5 changes to pale-yellow colors when S and Te are loaded. With Se loading, on the other hand, the zeolite changes to orange or brown. However, the color is not uniform, and in many cases the sample ends become denser. This spatial color variation seems to originate from some non-ideal pore structures of the present ZSM-5.

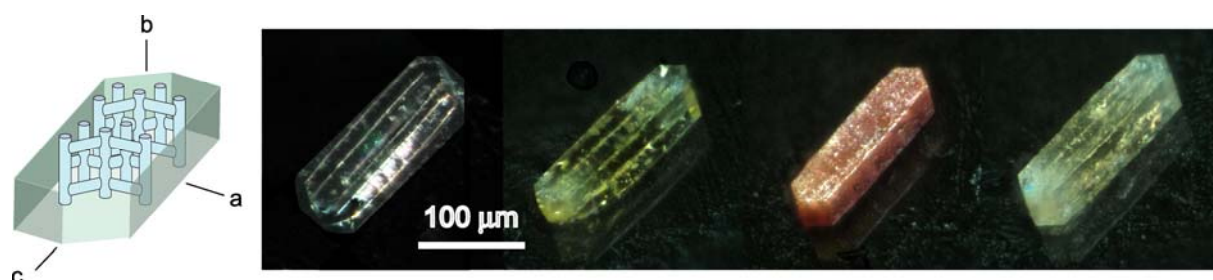


Fig. 3. An external view of employed ZSM-5 with the crystal directions and magnified channel structures, and photographs of ZSM-5, z-S, z-Se, and z-Te from the left to right-hand side.

Figure 4 compares transmission spectra of ZSM-5, z-S, z-Se, and z-Te. Corresponding to the photograph in Fig. 3, ZSM-5 exhibits high transmittance in this spectral region. The gradual transmittance decrease at shorter wavelengths may reflect slight light scattering. With the chalcogen loading, transparency at short wavelength regions is substantially reduced, which suggests an absorption arising from photo-electronic excitation. However, the spectra depend upon the chalcogen. The absorption edge of z-Se ($\sim 550 \text{ nm}$) appears to more red-shift than those ($\sim 400 \text{ nm}$) of z-S and z-Te. We also see that z-S and z-Te show clear transmission dips at $\sim 450 \text{ nm}$, which probably arise from absorption, not scattering.

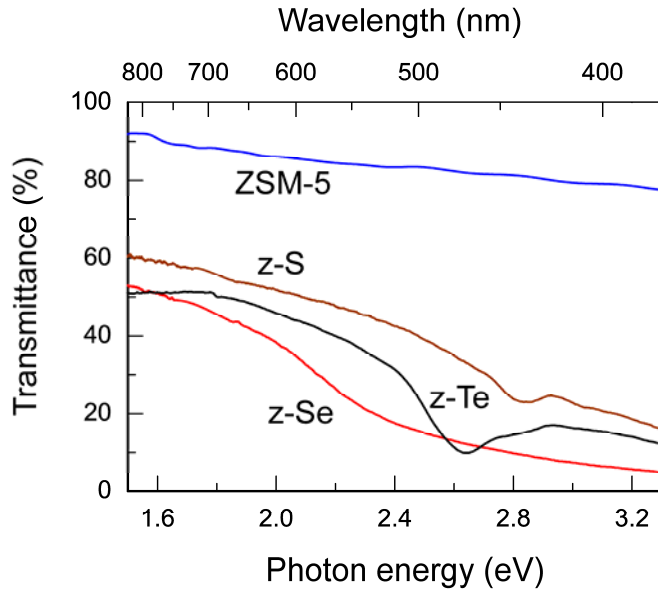


Fig. 4. Transmission spectra of ZSM-5, z-S, z-Se, and z-Te.

Figure 5 compares PL and absorbance spectra of the three materials. The PL is excited by light with several photon energies of 1.8 – 2.8 eV. The absorbance is calculated from the transmittance in Fig. 4. It is mentioned that, under the light excitation, template-desorbed ZSM-5 has produced no detectable PL. On the other hand, all the chalcogen-loaded samples provide broad PL in visible wavelengths at room temperature. Subsidiary experiments for all the samples have demonstrated that no PL peaks exist at near infrared regions up to a wavelength of $\sim 1.5 \mu\text{m}$.

Material dependence is interesting. In Fig. 5, the PL intensities on the vertical axis are normalized by the intensity of incident laser light. And, we see that z-S gives the strongest signal, z-Te the next, and z-Se the weakest by $\sim 1/200$ than that in z-S. It should be noted that this intensity variation cannot be correlated with the absorbed laser intensities. For instance, at 1.96 eV, z-S and z-Te are comparatively transparent to z-Se, while the PLs of the two are substantially stronger. Accordingly, we ascribe the intensity variation to a difference in the efficiency of radiative recombination. On the other hand, spectral features are also contrastive. All the PL spectra distribute at around 500–700 nm, or 1.6–2.6 eV. However, in z-S and z-Te, the strongest dark-red emissions are obtained under 1.96 eV excitation, while in z-Se an intense green emission is excited by 2.81 eV light. It should be underlined that, at least for z-Se, the so-called half-gap rule [27], i.e. the PL peak in chalcogenide glasses being located at $\sim E_g/2$ (E_g is an optical gap), is totally suppressed.

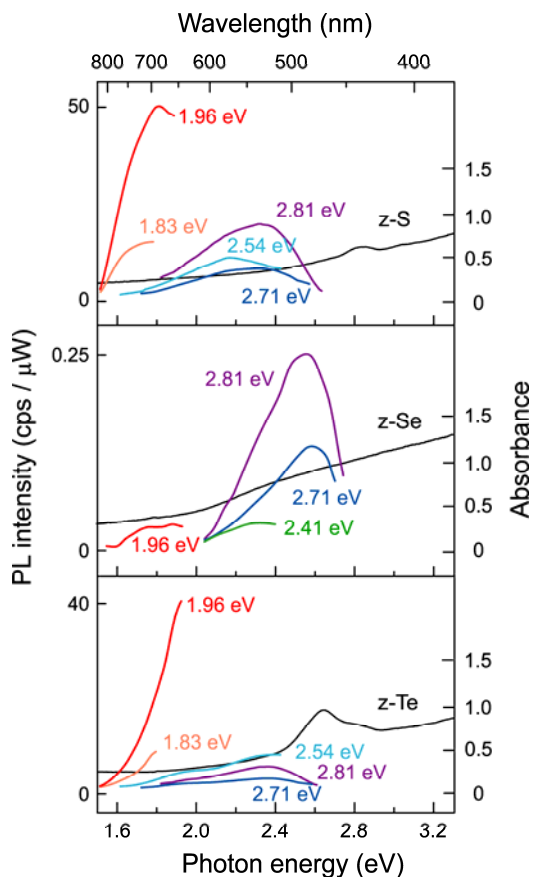


Fig. 5. Photoluminescence and absorbance spectra of z-S, z-Se, and z-Te at room temperature. The left-hand side vertical axis is scaled in luminescence intensity (cps) normalized by excitation light intensity (μW).

4. Discussion

Fig. 1 gives valuable insight into the sizes of pore diameters in ZSM-5 and of plausible guests. The framework and free diameters of the channels in ZSM-5 are reported to be ~ 0.83 nm and ~ 0.56 nm [25], which are greater than van-der-Waals atomic diameters of S, Se, and Te, which are 0.37, 0.40, and 0.44 nm, respectively [28]. This implies that, all the single atoms and dimmers of the chalcogens can penetrate into the channel. Trimers may also penetrate, if the shape is nearly straight, a possibility being suggested theoretically [29]. On the other hand, the pore diameters are comparable to the smallest sizes of stable molecules of these atoms. That is, the framework diameter of a S_8 ring molecule is ~ 0.47 nm [21], the framework cross-section diameters of Se and Te helices are 0.20 nm [22, 23] and 0.23 nm [22]. Accordingly, the van-der-Waals diameters of these molecules are estimated at ~ 0.8 nm, ~ 0.6 nm, and ~ 0.7 nm, respectively. We, therefore, envisage that only Se chains may penetrate into the zeolite pores. In contrast, penetration of S_8 molecules and Te chains seems difficult, while small clusters such as dimmers and trimers may be able to penetrate into the pores in ZSM-5.

Comparison with previous data could be also valuable. For the most common forms of crystalline S, Se, and Te, the optical gaps are reported to be ~ 4 [21], ~ 1.9 eV [30], and ~ 0.33 eV [31]. We then see some

correspondences between these gaps and the present absorption edges for z-S (~ 3 eV) and z-Se (~ 2.2 eV), while a discrepancy (~ 0.33 and 3 eV) for Te is remarkable. Otherwise, we may survey related data for small chalcogen clusters. For S, Averkiev et al. [7] reports for S-loaded NaA zeolite three absorption bands at $2\text{--}3$ eV, attributing to S_3 and S_4 clusters, which is consistent with results obtained by Meyer et al. for red S [32]. For Se, Poborochii reports that Se-loaded cancrinite shows an absorption peak at ~ 3 eV and a PL peak at ~ 1.5 eV at 77K, which are attributed to Se_2 ions [16]. Te in mordenite shows an absorption edge at ~ 1 eV [9], and PL of Te_2 is reported to appear at 2.2 eV [33].

Taking these previous results into account, we envisage different forms for the three chalcogens in ZSM-5. S and Te seem to have forms of short chains such as dimmers and trimmers. On the other hand, Se takes relatively-long chains with atomic numbers of ~ 100 . This model is consistent with the absorption spectra. For z-S, it seems that S_2 governs the absorption edge at ~ 3 eV [7, 32] and an absorbance peak at ~ 2.8 eV arises from S_3 chains. For Se, single chains can be geometrically incorporated into the ZSM-5 pores. Accordingly, the blue-shifted absorption edge of ~ 2.2 eV from ~ 1.9 eV in trigonal Se can be ascribed to disappearance of inter-chain interaction [10, 29] and to a quantum-well effect. For Te, Te_2 and Te_3 seem to be the most plausible candidates for interpreting the edge at ~ 3 eV and the peak at ~ 2.6 eV [33]. However, for elucidation, we need theoretical calculations for small Te clusters. The present model is also consistent with the variation of PL intensities, which can be ascribed to the efficiencies of radiative recombination. Since the recombination efficiency tends to decrease with an increase in cluster size, due to wider carrier diffusion and so forth [34], Se chains provide the weakest signal. On the other hand, the small clusters of S and Te can be regarded as kinds of inorganic dyes.

Alternatively, we may ascribe the peaks at ~ 2.7 eV and the similar PL features in S and Te to some defects in ZSM-5 matrix which are produced by the chalcogen incorporation. For instance, S and Te may react with O atoms in ZSM-5, producing defects, which have similar structures to the so-called oxygen-deficient center in SiO_2 [35], which is known to provide an absorption and PL peak at ~ 2.8 eV. Nevertheless, this idea is difficult to interpret the intense PLs excited by 1.96 eV light. The first idea is more plausible.

5. Conclusions

Optical properties of chalcogen-loaded ZSM-5 have been comparatively investigated. Intense visible PL and absorption peaks are observed for S and Te at room temperature. Se loading produces the most dense-colored samples, while the PL is the weakest. These observations suggest that S and Te are incorporated as small clusters such as dimmers, while Se is loaded as relatively-long chain fragments.

Acknowledgements

The authors would like to thank Drs. Y. Kiyozumi for supplying ZSM-5 samples, A. V. Kolobov and V. V. Poborochii for unpublished information, and graduate students, S. Okamoto and K. Noda. The authors also acknowledge a financial support from Nippon Sheet Glass Foundation for Material Science and

References

- [1] H.S. Nalwa (ed.) Handbook of Advanced Electronic and Photonic Materials and Devices Vol. 6, Academic Press, San Diego, 2001.
- [2] <http://www.iza-structure.org/databases/>
- [3] J. Sauer, F. Marlow, F. Schüth, in: H.S. Nalwa (ed.), Handbook of Advanced Electronic and Photonic Materials and Devices Vol. 6, Academic Press, San Diego, 2001, Chapter 5, pp 153-171.
- [4] S.A. Averkiev, L.S. Agroskin, V.G. Aleksandrov, V.N. Bogomolov, Yu.N. Volgin, A.I. Gutman, T.B. Zhukova, V.P. Petranovskii, D.S. Poloskin, L.P. Rautian, S.V. Kholodkevich, Sov. Phys. Solid State 20 (1978) 251-253.
- [5] H. Garcia, H. D. Roth, Chem. Rev. 102 (2002) 3947-4007.
- [6] B. Smit, T.L.M. Maesen, Nature 451 (2008) 671-678.
- [7] S. A. Averkiev, L. S. Agroskin, V. G. Aleksandrov, V. N. Bogomolov, Yu. N. Volgin, A. I. Gutman, T. B. Zhukova, V. P. Petranovskii, D. S. Poloskin, L. P. Rautian, and S. V. Kholodkevich, Sov. Phys. Solid State 20 (1978) 251-253.
- [8] V.N. Bogomolov, A.I. Zadorozhnyi, V.P. Petranovskii, A.V. Fokin, S.V. Kholodkevich, JETP Lett. 29 (1979) 373-375.
- [9] V.N. Bogomolov, S.V. Kholodkevich, S.G. Romanov, L.S. Agroskin, Solid State Commun. 47 (1983) 181-182.
- [10] Y. Katayama, M. Yao, Y. Ajiro, M. Inui, H. Endo, J. Phys. Soc, Jpn. 58 (1989) 1811-1822.
- [11] Y. Nozue, T. Kodaira, O. Terasaki, K. Yamazaki, T. Goto, D. Watanabe, J.M. Thomas, J. Phys.: Condens. Matter 2 (1990) 5209-5217.
- [12] K. Matsuishi, T. Isome, J. Ohmori, S. Onari, T. Arai, Phys. Stat. Sol. (b) 215 (1999) 301-306.
- [13] L. He, Z.X. Shen, G. Gu, L. Qin, S.H. Tang, Chem. Phys. Lett. 300 (1999) 504-508.
- [14] A.V. Kolobov, H. Oyanagi, V.V. Poborchii, K. Tanaka, Phys. Rev. B59 (1999) 9035-9043.
- [15] V.V. Poborchii, J. Chem. Phys. 114 (2001) 2707-2717.
- [16] V.V. Poborchii, G.-G. Lindner, M. Sato, J. Chem. Phys. 116 (2002) 2609-2617.
- [17] P. Simoncic, T. Armbruster, Microporous and Mesoporous Mater. 71 (2004) 185-198.
- [18] A. Goldbach, L.E. Iton, M. Grimsditch, M.L. Saboungi, Chem. Mater. 16 (2004) 5104-5113.
- [19] I.L. Li, S.C. Ruan, Z.M. Li, J.P. Zhai, Z. K. Tang, Appl. Phys. Lett. 87 (2005) 71902-71905.
- [20] A. Ikawa, H. Fukutome, J. Phys. Soc. Japan 59 (1990) 1002-1016.
- [21] W.R. Salaneck, N.O. Lipari, A. Paton, R. Zallen, and K.S. Liang, Phys. Rev. B12 (1975) 1493-1500.
- [22] R.M. Martin, G. Lucovsky, Phys. Rev. B13 (1976) 1383-1395.
- [23] P. Andonov, J. Non-Cryst. Solids 47 (1982) 297-339.
- [24] G.T. Kokotailo, S.L. Lawton, D.H. Olson, and W.M. Meier, Nature 272 (1978) 437-438.

- [25] H. van Koningsveld, J.C. Jansen, H. van Bekkum, *Zeolites* 10 (1990) 235-242.
- [26] S. Shimizu, H. Hamada, *Microporous and Mesoporous Mater.* 48 (2001) 39-46.
- [27] R. A. Street, *Adv. Phys.* 25 (1976) 397-454.
- [28] L. Pauling, *The nature of the chemical bond and the structure of molecules and crystals: an introduction to modern structural chemistry*, Cornell University Press, Ithaca, New York, 1960, p 260.
- [29] T. Yamaguchi, F. Yonezawa, *J. Non-Cryst. Solids* 156-158 (1993) 268-271.
- [30] G.G. Roberts, S. Tutihasi, R.C. Keezer, *Phys. Rev.* 166 (1968) 637-643.
- [31] S. Tutihasi, G.G. Roberts, R.C. Keezer, R.E. Drews, *Phys. Rev.* 177 (1969) 1143-1150.
- [32] B. Meyer, M. Gouterman, D. Jensen, T.V. Oommen, K. Spitzer, T. Stroyer-Hansen, *Sulfur Research Trends* (American Chemical Soc., Washington, D. C., 1972) pp. 53-72.
- [33] G.-G. Lindner, K. Witke, H. Schlaich, and D. Reinen, *Inorganic Chimica Acta* 252 (1996) 39-45.
- [34] S. Takeoka, *Phys. Rev. B* 58 (1998) 7921-7925.
- [35] L. Skuja, *J. Non-Cryst. Solids* 239 (1998) 16-48.

Figure captions

Fig. 1. A list of zeolite of interest and chalcogen. In the lower part, the zeolite is specified by the Al/Si ratio (or Al/P for $\text{AlPO}_4\text{-5}$) and the free pore diameter with symbols representing conformation dimensions of pore structures; a spherical cavity by a circle, one-dimensional channels by rectangles, a two- by a square, and the three- by triangles. In the upper part, van-der-Waals diameters of chalcogen atoms (circles) and sizes of related molecules are depicted. For S, a framework diameter of S_8 ring molecule is plotted with an attached bar extending to an approximate size taking a van-der-Waals atomic diameter into account. For Se and Te, framework cross-sectional diameters of the three-fold helices in trigonal crystals are plotted with the bars to the van-der-Waals diameters.

Fig. 2. Infrared spectra of as-received and template-desorbed ZSM-5 and z-Se.

Fig. 3. An external view of employed ZSM-5 with the crystal directions and magnified channel structures, and photographs of ZSM-5, z-S, z-Se, and z-Te from the left to right-hand side.

Fig. 4. Transmission spectra of ZSM-5, z-S, z-Se, and z-Te.

Fig. 5. Photoluminescence and absorbance spectra of z-S, z-Se, and z-Te at room temperature. The left-hand side vertical axis is scaled in luminescence intensity (cps) normalized by excitation light intensity (μW).

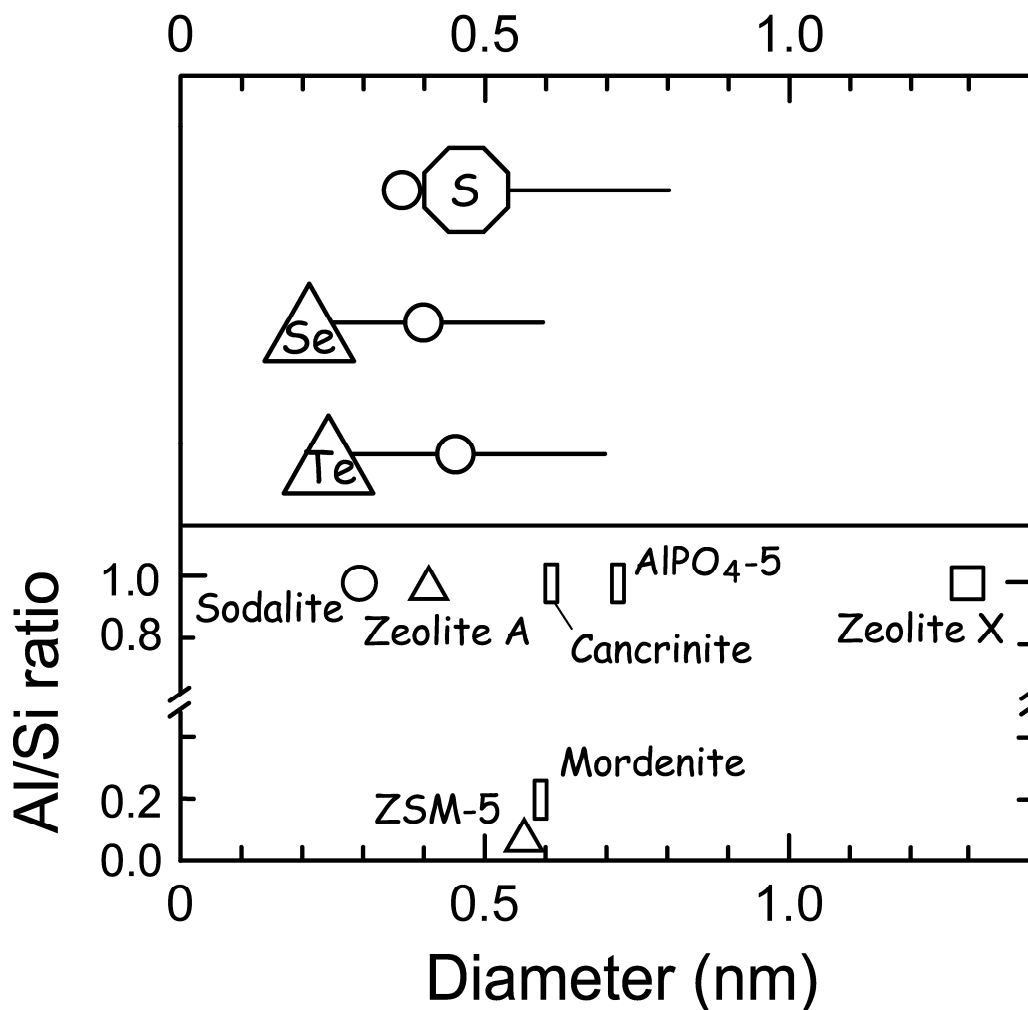


Fig. 1. A list of zeolite of interest and chalcogen. In the lower part, the zeolite is specified by the Al/Si ratio (or Al/P for AlPO₄-5) and the free pore diameter with symbols representing conformation dimensions of pore structures; a spherical cavity by a circle, one-dimensional channels by rectangles, a two- by a square, and the three- by triangles. In the upper part, van-der-Waals diameters of chalcogen atoms (circles) and sizes of related molecules are depicted. For S, a framework diameter of S₈ ring molecule is plotted with an attached bar extending to an approximate size taking a van-der-Waals atomic diameter into account. For Se and Te, framework cross-sectional diameters of the three-fold helices in trigonal crystals are plotted with the bars to the van-der-Waals diameters.

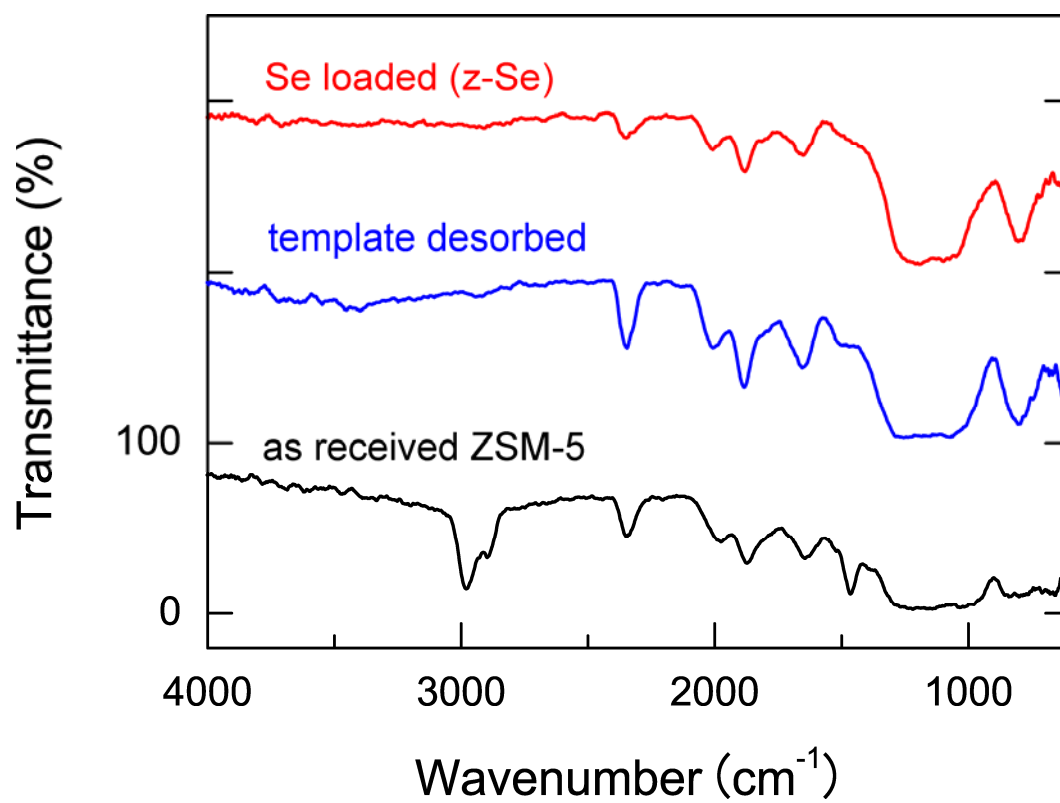


Fig. 2. Infrared spectra of as-received and template-desorbed ZSM-5 and z-Se.

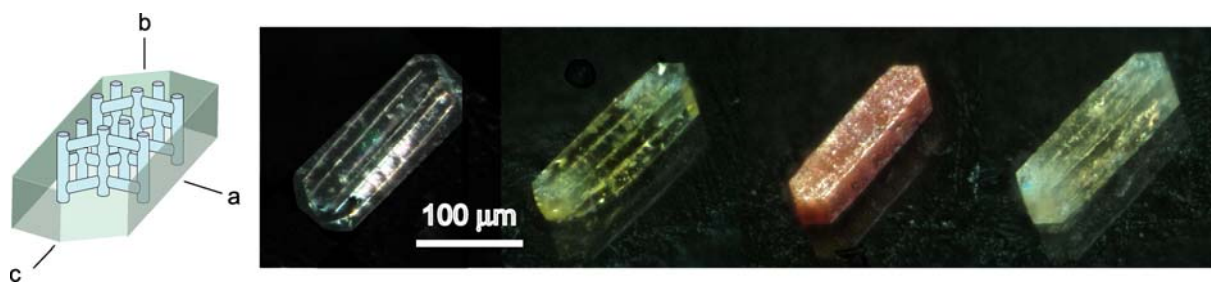


Fig. 3. An external view of employed ZSM-5 with the crystal directions and magnified channel structures, and photographs of ZSM-5, z-S, z-Se, and z-Te from the left to right-hand side.

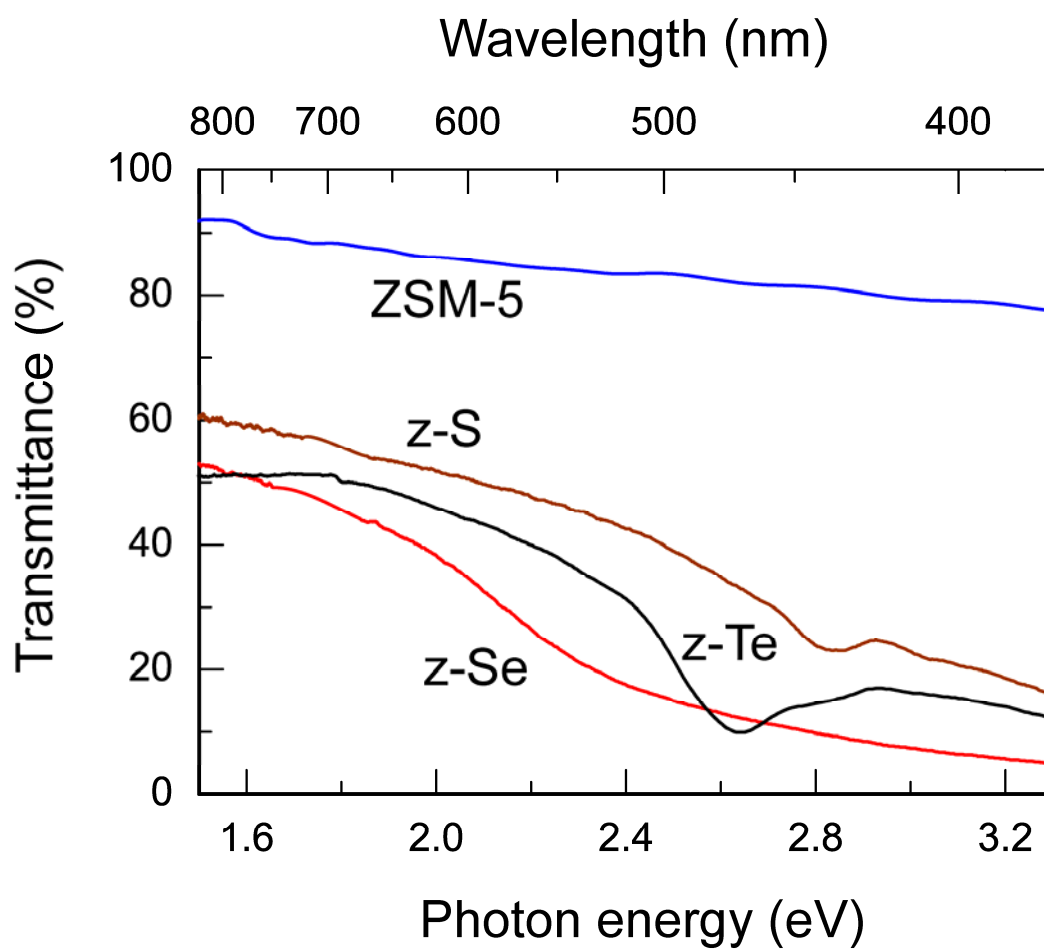


Fig. 4. Transmission spectra of ZSM-5, z-S, z-Se, and z-Te.

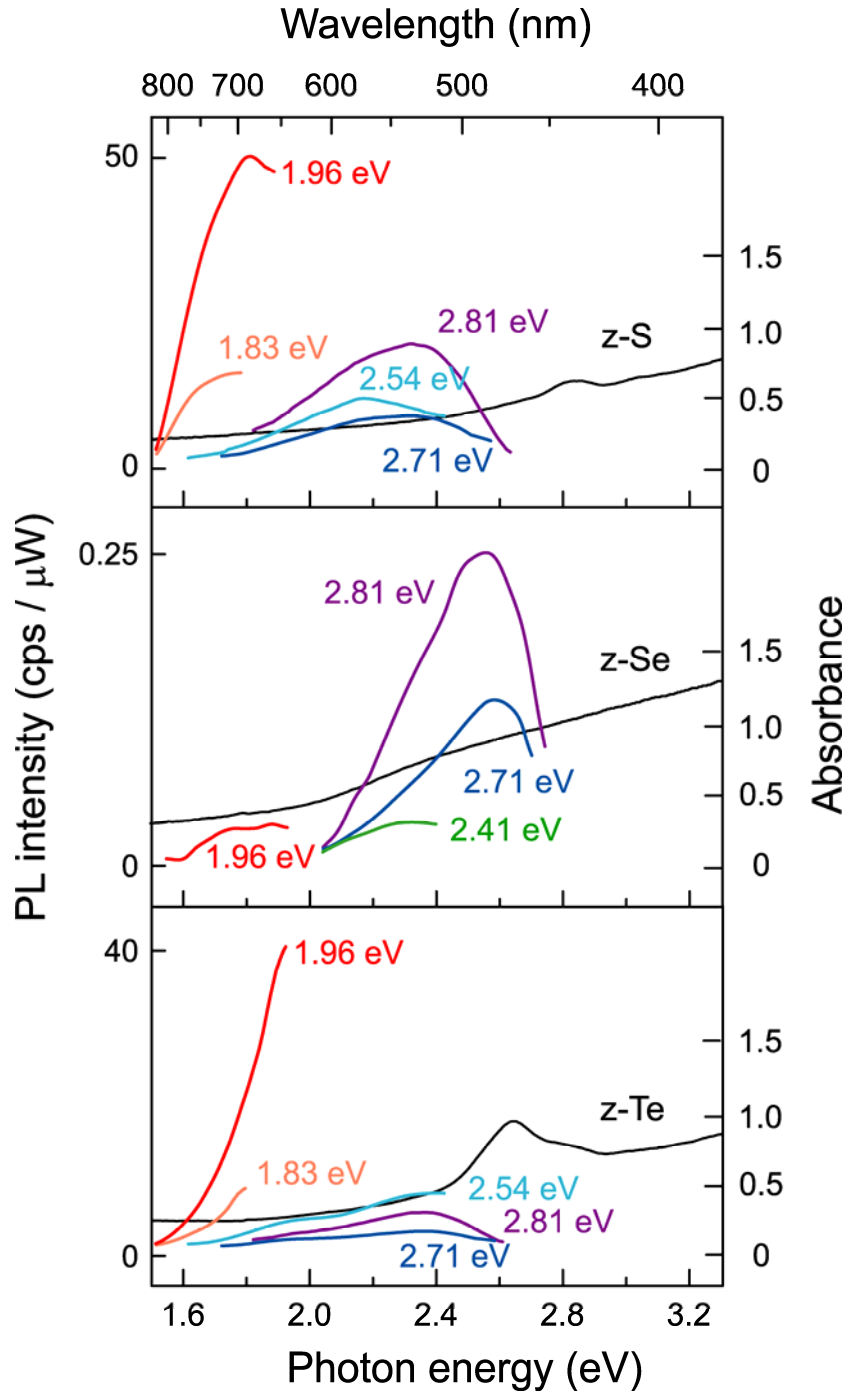


Fig. 5. Photoluminescence and absorbance spectra of z-S, z-Se, and z-Te at room temperature. The left-hand side vertical axis is scaled in luminescence intensity (cps) normalized by excitation light intensity (μW).